Supporting Information

Trigo et al. 10.1073/pnas.1209798109

SI Materials and Methods

General Procedures. Rats (Sprague–Dawley, aged 11–17 d) were decapitated under isoflurane anesthesia following approved ethical procedures. Sagittal slices 200 μm thick were cut with a vibroslicer (VT1200S; Leica) in ice-cold artificial cerebrospinal fluid (ACSF), stored at 35 °C for 1 h, and subsequently kept in the same solution at room temperature until use. The solution for cutting, storing slices, and recording comprised the following: 115 mM NaCl, 2.5 mM KCl, 26 mM $NaHCO_3$, 1.3 mM NaH_2PO_4, 25 mM glucose, 2 mM $CaCl_2$, and 1 mM $MgCl_2$, with osmolality adjusted to 300 mOsm/kg, pH 7.4 when gassed with 5% (vol/vol) CO_2 and 95% (vol/vol) O_2.

Electrophysiology. Molecular layer interneurons (MLIs) were voltage-clamped with the whole-cell patch-clamp technique (Axopatch 200A or 200B amplifier; Molecular Devices). The composition of internal solution (IS) used for the postsynaptic cell was as follows: 150 mM KCl, 1 mM EGTA, 10 mM Hepes, 0.1 mM $CaCl_2$, 4.6 mM $MgCl_2$, 4 mM Na_2ATP, 0.4 mM NaGTP, and 0.04 mM Alexa 488. The presynaptic IS in early experiments was as follows: 110 mM KCl, 20 mM Hepes, 0.5 mM $MgCl_2$, 4.25 mM $CaCl_2$, 5 mM Na_2ATP, 0.5 mM NaGTP, 5 mM KOH, 5 mM 1-(2-nitro-4,5-dimethoxyphenyl)-N,N,N′,N′-tetrakis[(oxycarbonyl)methyl]-1,2-ethanediamine (DM-nitrophen), 0.08 mM Alexa 594, 0 or 1 mM Oregon Green Bapta-5N (OGB-5N), and 10 mM GABA. In later experiments, Hepes buffer was increased to 50 mM: 100 mM KCl; 50 mM Hepes; 0.5 mM $MgCl_2$; 4.25 mM $CaCl_2$; 5 mM Na_2ATP; 0.5 mM NaGTP; 5 mM KOH; 5 mM DM-nitrophen; 0.08 mM Alexa 594; 10 mM GABA; 0, 0.5, or 1 mM OGB-5N; and 0, 0.1, or 1 mM EGTA. IS had a pH of 7.3 and an osmolality of ≈300 mOsm/kg. Recordings were made at room temperature (20–22 °C). The calculated junction potential of 3 mV was not corrected. Pipette resistance was 5 MΩ. Series resistance was 20.0 ± 5.6 MΩ (range: 12–31 MΩ) and was not compensated. Holding potentials were usually −60 mV in both presynaptic and postsynaptic neurons. Synaptic connectivity was tested by depolarizing voltage steps (2 to 3 ms to 0 mV) applied to the presumptive presynaptic cell. Recordings were filtered at 5 kHz, digitized at 16.7 kHz with a Power 1401 interface (Cambridge Electronic Design), and acquired with WinWCP (developed by John Dempster, University of Strathclyde, Glasgow, Scotland). Data were analyzed in Igor Pro (Wavemetrics).

Most data were obtained from cells located in the proximal part of the molecular layer (basket cells). However, interneurons located in the distal molecular layer (stellate cells) were also included.

Photolysis of DM-Nitrophen. Photolysis of DM-nitrophen was implemented here at 405 nm in a custom microscope based around a 63×/0.9-N.A. water dipping objective (Leica). Light from a diode laser (Iflex 2000 405 nm; Point Source or DeepStar 405; Omicron) was focused as a 5-μm, 3-μm, or 1-μm diameter spot in the microscope field, viewed with an electron multiplying charge-coupled device (EM CCD) camera at 0.25 μm per pixel (Ixon, 512 × 512 pixels; Andor Technology). The calibration of laser photolysis and additional details of the microscope are given elsewhere (1).

DM-nitrophen was synthesized by Gordon P. Reid (Medical Research Council, National Institute for Medical Research, London) following the procedures of Ellis-Davies and Kaplan (2, 3) with purification by anion exchange chromatography on DEAE cellulose (triethylammonium salt) and Dowex cation exchange to isolate as the sodium salt. The compositions of DM-nitrophen–containing intracellular solutions used in the presynaptic recording were calculated in Mathcad (Parametric Technology Corporation) based on published affinity constants for the competing Ca^{2+} and Mg^{2+} chelators present. During DM-nitrophen photolysis, two protons are absorbed for each Ca^{2+} ion released. To minimize the alkalinization on photolysis, high concentrations of presynaptic Hepes were used, 20 mM in initial experiments and 50 mM in later experiments. Controls to test the effects of intracellular alkalinization on synaptic release by adding NH_4Cl extracellularly showed no effect up to 5 mM NH_4Cl, corresponding to 2.5 mM Ca release from DM-nitrophen.

Although fast-rising, large-amplitude responses similar to spontaneous synaptic events were typically seen, local DM-nitrophen photolysis occasionally evoked a different class of postsynaptic currents (PSCs), with small peak amplitude (<50 pA) and slow rise time (time to peak: 5–10 ms). These were attributed to GABA spillover originating from synapses with MLIs distinct from the recorded "postsynaptic" MLI. They were not included for data analysis.

Fluorescence Imaging. Epifluorescence excitation was by light-emitting diodes in a dual lamp-house (Optoled; Cairn Research) at 470/40 nm and 572/35 nm excitation and fluorescence emitted at 520/40 nm and 630/60 nm was detected with an EM CCD camera (Ixon, with filters from Chroma). To reconstruct morphology with Alexa 488 and Alexa 594, single full frames were taken, varying the focal depth. ImageJ (National Institutes of Health; http://rsbweb.nih.gov/ij/index.html) was used to make the stacks (at 1-μm increments) and composite images. Cell reconstruction was with The Gimp.

Calcium Imaging. The low-affinity indicator OGB-5N [K(Ca) = 37 μM] was used at 1 mM to monitor changes of Ca^{2+} on photolysis. A subregion of the CCD comprising sixteen 4 × 4 binned pixels, giving a resolution of 1 μm, was imaged in 1.8-ms exposures at 300 Hz. Fluorescence was corrected for background, determined in pixels at the periphery of the subregion. All traces shown are single sweep responses without averaging. $\Delta F/F_0$ was calculated in the central region containing the laser spot and axon. When necessary, a correction was applied for slow bleaching by fitting a sum of two exponential terms.

Data Analysis. The latency of each synaptic event from the time of the laser pulse (or the first pulse in a train) was measured by visual inspection and cursors in the digitized records. A probability density function (pdf) of two exponential components was fitted to the intervals by maximum likelihood to estimate the mean intervals and the number of events in each exponential component. The use of maximum likelihood to fit randomly distributed time intervals is discussed by Colquhoun and Sigworth (4). For display, the pdfs were scaled by the number of events and bin width and superimposed on the histograms of latencies. Errors for the parameters were calculated as 0.5-log likelihood intervals. The maximum likelihood fits and error estimates were made on unbinned intervals with program EKDist (included in DCProgs, developed by D. Colquhoun and I. Vais; available at www.onemol.org.uk) after data conversion to SCAN format with Python script (R.Lape; code.google.com/p/dc-pyps).

Statistical comparisons between different groups were with a nonpaired Wilcoxon rank-sum test. The level of significant difference was established at $P < 0.05$. Data are presented as mean ± SD. The term n represents the number of independent measurements.

Correction for Missed Events. The slow activation and high occupancy of postsynaptic receptors during quantal events at MLI-MLI synapses [which vary from site to site, with a mean of 77% (5, 6)]

may result in closely spaced events being missed at high frequencies of exocytosis. It was necessary to calculate the fraction of missed events and apply a correction to the average number of quanta observed in response to each laser stimulation.

We first estimated the dead-time between resolvable consecutive events by inspecting the data for closely separated events and by simulating consecutive GABAergic quanta at different occupancies and interpulse intervals. The dead-time between resolvable consecutive events was estimated at 0.6 ms.

The fraction of events that would be missed was based on the distribution of first latencies (Fig. 5*A*, *Bottom*). First latencies can be measured precisely, with a resolution of 100 μs, and unambiguously in the data. The correction is for missed second and subsequent events that occur during the "dead-time" following the preceding event. Assuming that successive events are independent, the probabilities of two or more events occurring in successive 0.6-ms intervals (the dead-time) were calculated as the product of the individual probabilities in the two bins. These, in turn, were estimated from the first latency histogram as the normalized frequencies obtained in 0.6-ms bins, and the products were summed over the 10-ms burst time. If the number of quanta available is small and replaced slowly on the time scale of the burst, as apparent here, the probability of second and subsequent release is reduced because fewer vesicles are available. The fraction missed when two quanta are available is approximately half of that for release from an infinite pool, and for three, four, and five available quanta, intermediate values are obtained.

With a dead-time of 0.6 ms, the fraction of missed events was estimated as 7% for two vesicles available for release. Thus, the "ready releasable pool" (RRP) is corrected in this way from the mean uncorrected value of 1.76–1.9. The fraction of events missed increased if longer dead-times were applied up to a maximum of 20% at 2 ms for a large pool of vesicles, which was reduced to 10% when two vesicles are available. The calculations based on the observed first latencies indicate that the fraction of events missed because of postsynaptic receptor saturation is small.

To check this correction further, and to see whether the statistics of release were verified, we simulated release from a single active zone with three independent docking sites as in the cartoon in Fig. 5*C*. Each docking site was assigned an occupancy of 0.7, release was described by a single rate constant of 250 s^{-1}, and the dead-time was set at 0.6 ms. This gave an estimated fraction of missed events of 8.5%, similar to the correction applied above.

Occupancy of Postsynaptic Receptors. The postsynaptic receptor occupancy was calculated as described by Auger and Marty (5). Briefly, assuming that there is no receptor recovery after the first release event, the receptor occupancy (ω) by the first quantum can be calculated from

$$A_2/A_1 = 1 - \omega,$$

where A_2 and A_1 are the amplitudes of the second and first components, respectively, in a double PSC.

Drugs. All the drugs used were from Sigma–Aldrich, Invitrogen, or Tocris Biosciences.

Lack of Effect of Internal Alkalinization on Evoked Synaptic Currents. Photoactivation of DM-nitrophen leads to the consumption of two protons for each Ca^{2+} released; hence, transient internal alkalinization occurs in the presynaptic terminal that may not be adequately buffered by the slow CO_2-bicarbonate buffer or by the neuronal buffering capacity. Here, initial experiments were conducted with 20 mM internal Hepes and later experiments were conducted with 50 mM internal Hepes. The two sets of data were analyzed separately and found not to differ in the distribution of latencies, and they were combined in the final analyses presented.

To test directly for effects of alkalinization on synaptic GABA release, we compared synaptic currents at MLI-MLI synapses before and after addition of NH_4Cl to the bath, which produces a stoichiometric alkalinization by intracellular protonation of the membrane-permeable NH_3. The experiments were performed with 10 mM Hepes-buffered ACSF (pH 7.4). Evoked events (two stimuli with a 30-ms interval, every 5 s) were recorded in control conditions and during the addition of 5 mM NH_4Cl. Neither the peak amplitude (mean ratio in NH_4Cl vs. control: 0.90 ± 0.11, $n = 4$) nor the value of the paired pulse ratio (mean ratio in NH_4Cl vs. control: 0.89 ± 0.22, $n = 4$) was significantly altered by NH_4Cl superfusion ($P > 0.05$, Wilcoxon signed rank test). These experiments indicate that the effects described in the present work are not due to changes in intraterminal pH and, further, that release is relatively insensitive to alkalinization.

Release Statistics for Separate Docking Sites. We assume here that a single synaptic release site possesses several independent docking sites, where vesicles must bind before exocytosis (Fig. 5*C*). The number of vesicles, *r*, released in response to a given stimulus strength, *s*, is related to the number of docking sites, N_D, by the equation

$$r = N_D * f * s,$$

where *f* and *s* are random variables varying from 0 to 1, respectively, representing the fraction of the sites occupied and the probability for one occupied site to undergo exocytosis in response to the high calcium stimulus.

Release or failure is described by a binomial with time-averaged mean number released $\langle r \rangle = N_D * P$ and variance $var(r) = N_D * P * (1 - P)$. The binomial *P* in this formulation represents the product $F * S$, where *F* and *S* are the mean values of *f* and *s*, respectively.

The RRP is the value of *r* when *S* is maximal ($S = 1$) and depends on the product $RRP = N_D * f$. An estimate of *F* can be found from the ratio of the mean *r* to the maximum value seen in a run at the same stimulus strength: $\langle r \rangle / r(max) = (N_D * F) / N_D = F$.

The binomial model predicts a coefficient of variation (CV) equal to

$$CV_B = (\mathrm{var}(r))^{1/2} / \langle r \rangle = (\langle r \rangle (1-P))^{1/2} / \langle r \rangle = ((1-P)/\langle r \rangle)^{1/2} = ((1 - \langle r \rangle / r(max)) / \langle r \rangle)^{1/2}.$$

On the other hand, a Poisson model predicts a CV of

$$CV_P = (\mathrm{var}(r))^{1/2} / \langle r \rangle = \langle r \rangle^{1/2} / \langle r \rangle = \langle r \rangle^{-1/2}.$$

Stacks of Images of the Morphology of Neurons in Experiments Used for the Figures. Avi files containing stacks of images are available for all experiments illustrated (Movies S1, S2, S3, S4, S5, and S6).

1. Trigo FF, Corrie JET, Ogden D (2009) Laser photolysis of caged compounds at 405 nm: Photochemical advantages, localisation, phototoxicity and methods for calibration. *J Neurosci Methods* 180(1):9–21.
2. Kaplan JH, Ellis-Davies GC (1988) Photolabile chelators for the rapid photorelease of divalent cations. *Proc Natl Acad Sci USA* 85(17):6571–6575.
3. Ellis-Davies GC, Kaplan JH (1988) A new class of photolabile chelators for the rapid release of divalent cations: Generation of caged Ca and caged Mg. *J Org Chem* 53:1966–1969.
4. Colquhoun D, Sigworth FJ (1995) Analysis of single ion channel data. *Single Channel Recording*, eds Sakmann B, Neher E (Plenum, New York), 2nd Ed, pp 483–587.
5. Auger C, Marty A (1997) Heterogeneity of functional synaptic parameters among single release sites. *Neuron* 19(1):139–150.
6. Auger C, Kondo S, Marty A (1998) Multivesicular release at single functional synaptic sites in cerebellar stellate and basket cells. *J Neurosci* 18(12):4532–4547.

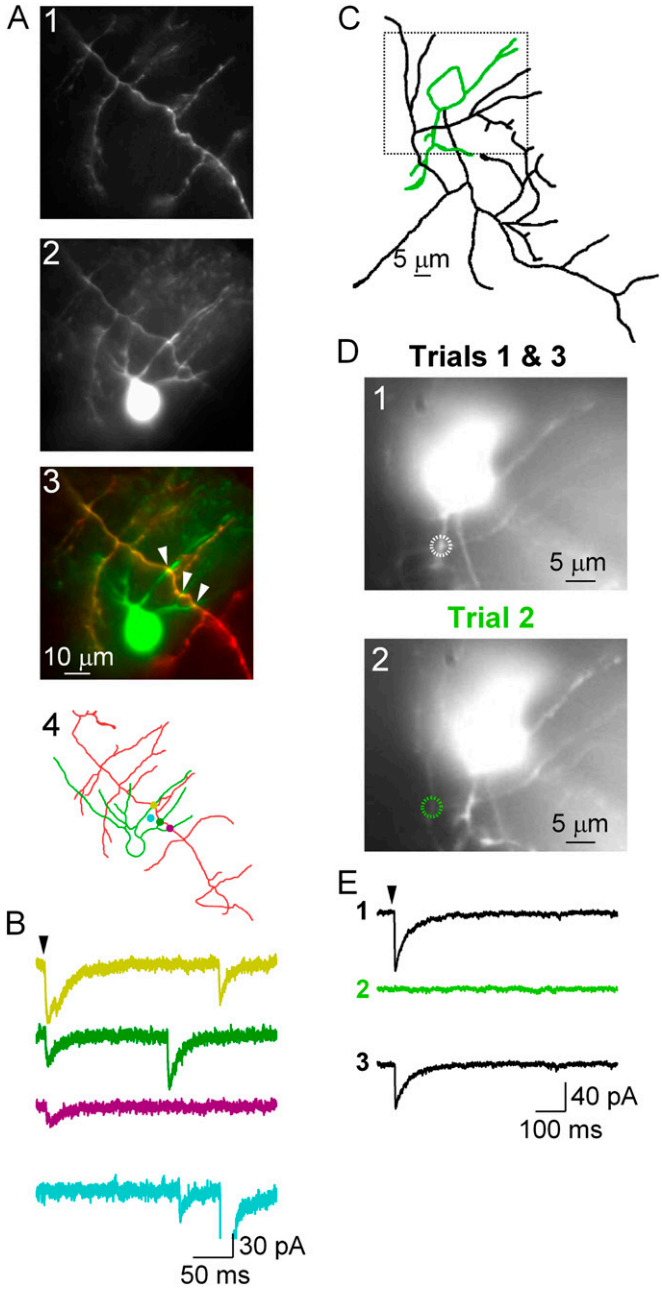

Fig. S1. Identification of synaptic release sites. (*A1*) Fluorescence image obtained under amber (572 nm) illumination. Only the Alexa 594-filled presynaptic cell can be seen. (*A2*) Fluorescence image obtained under blue (470 nm) illumination. Both Alexa 488 and Alexa 594 are excited. With this configuration, turning the blue light on and off and leaving the amber light on distinguished unambiguously the presynaptic cell from the postsynaptic cell. (*A3*) Superimposition of *A1* and *A2* with pseudocolors. The synaptic contacts that gave a PSC when stimulated with the laser spot are shown by arrowheads (PSCs are shown in *B*). The soma of the presynaptic cell is in the top left corner, out of the field of view. (*A4*) Reconstruction of the pair shown. The presynaptic axon is shown in red, and the postsynaptic cell is shown in green (Movie S1). (*B*) Laser-evoked currents obtained in four different places, marked with dots in *A4*. In this pair, three synaptic contacts could be identified. When the laser spot was moved to the position indicated by the blue dot, no PSC was evoked (blue trace). The black arrowhead indicates the time of the laser pulse. Parameters of the laser stimulation are as follows: duration, 200 μs; energy, 0.18 μJ. (*C*) Reconstruction from an autapse, with the postsynaptic somatodendritic domain shown in green and the axon shown in black (Movie S4). (*D*) Magnified view of the contact area (dotted line rectangle in *C*) shows two locations on the presynaptic axon (*D1* and *D2*), located about 5 μm apart (dotted white and green circles). (*E*) One of the spots (white circle, trials 1 and 3) is responsive (laser pulse timing indicated by the black arrowhead), but the other is not (green circle, trial 2). The responsive spot corresponds to a site of close apposition between the presynaptic axon and a postsynaptic dendrite.

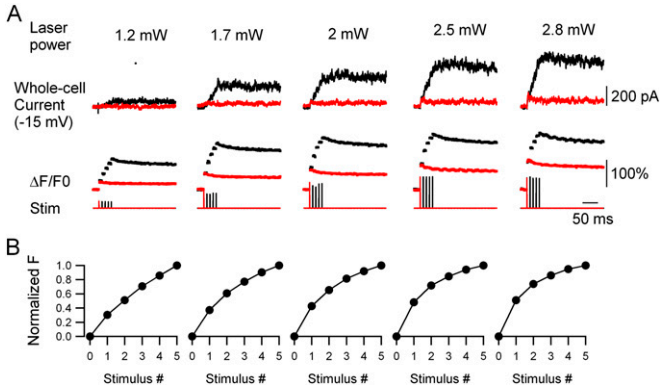

Fig. S2. Local Ca^{2+} release in MLI somata. (*A*) Short laser stimuli were applied to the soma of a MLI under voltage clamp at −15 mV, and the resulting OGB-5N fluorescence changes and Ca^{2+}-dependent K^+ currents (mostly due to BK channels) were recorded. Responses are shown to single pulses (red traces) and to trains of five pulses at 100 Hz (black traces; pulse duration, 0.1 ms; total laser energies, 0.12–1.4 μJ). Stim, stimulus. (*B*) Fluorescence amplitudes display a sublinear dependence on the number of applied stimuli (same laser power scale as in *A*), with approximate half-maximum occurring in response to two stimuli at 0.12 μJ per pulse and in response to one stimulus at 0.28 μJ.

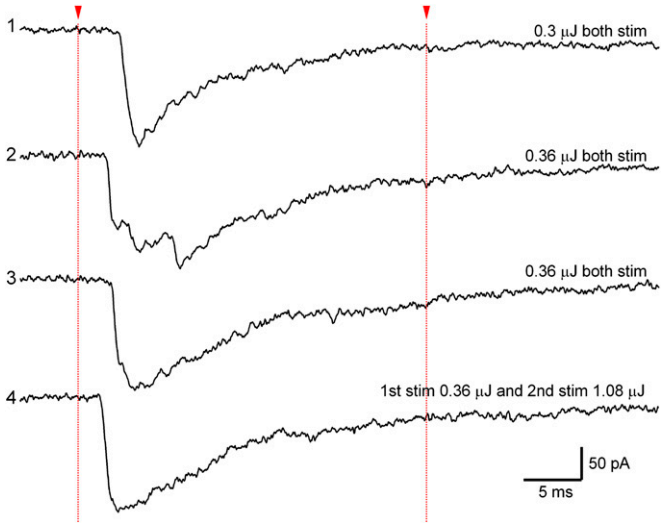

Fig. S3. PSCs in response to two successive stimuli (stim) in the same sweep. Records show laser-evoked PSCs (black traces) and times at which the laser pulses were delivered (red lines). Two brief laser pulses (0.1 ms) were delivered with a 30-ms interval to test whether the RRP had been fully depleted with the first pulse. The energy delivered by each pulse is indicated above each trace.

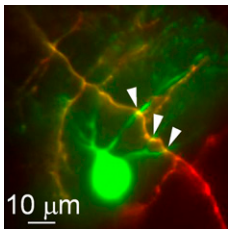

Movie S1. This movie corresponds to a z-stack of the pair shown in Fig. S1*A*.

Movie S1

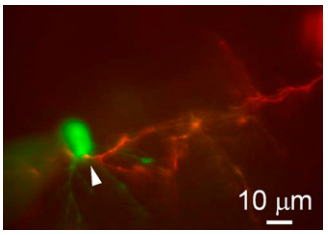

Movie S2. This movie corresponds to a z-stack of the pair shown in Fig. 1*B*.

Movie S2

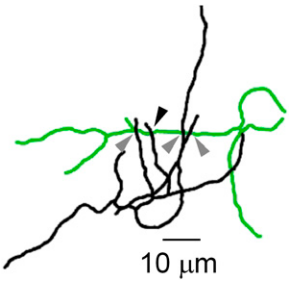

Movie S3. This movie corresponds to a z-stack of the autapse shown in Fig. 1*D*.

Movie S3

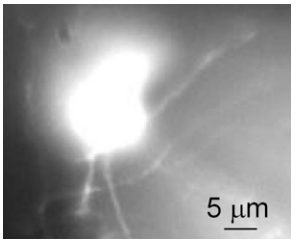

Movie S4. This movie corresponds to a z-stack of the autapse shown in Fig. S1*C*.

Movie S4

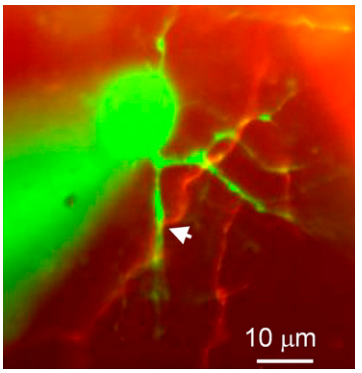

Movie S5. This movie corresponds to a z-stack of the pair shown in Fig. 3*A*.

Movie S5

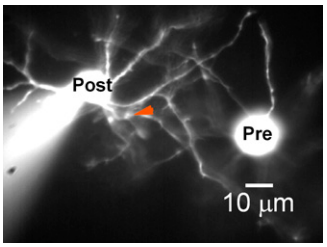

Movie S6. This movie corresponds to a z-stack of the pair shown in Fig. 4*A*.

Movie S6